Journal of Nuclear Medicine, published on November 9, 2017 as doi:10.2967/jnumed.117.190546

Thermal imaging is a non-invasive alternative to PET-CT for measurement of brown adipose tissue activity in humans

Authors: James Law[1], David E Morris[2], Chioma Izzi Engbeaya[3], Victoria Salem[3], Christopher Coello[4], Lindsay Robinson[1], Maduka Jayasinghe[3], Rebecca Scott[3], Roger Gunn[4], Eugenii Rabiner[4,5], Tricia Tan[3], Waljit S Dhillo[3], Stephen Bloom[3], Helen Budge[1], Michael E Symonds[1,6]*

Affiliations: [1]Early Life Research Unit, Division of Child Health, Obstetrics & Gynaecology, School of Medicine, University of Nottingham, United Kingdom. [2]Department of Electrical & Electronic Engineering, Faculty of Engineering, University of Nottingham, United Kingdom. [3]Division of Diabetes, Endocrinology and Metabolism, Imperial College, United Kingdom. [4]Imanova Centre for Imaging Sciences, Imperial College, London, United Kingdom. [5]Centre for Neuroimaging Sciences, King's College, London, United Kingdom. [6]Nottingham Digestive Disease Centre and Biomedical Research Centre, School of Medicine, University of Nottingham, United Kingdom.

***Corresponding Author:**

Prof Michael E Symonds,
The Early Life Research Unit,
Division of Child Health, Obstetrics and Gynaecology,
School of Medicine,
University Hospital,
University of Nottingham,
Nottingham, NG7 2UH United Kingdom
Telephone: +44 115 82 30611 Fax: +44 115 82 30626
Email: michael.symonds@nottingham.ac.uk

First Author:

Dr James M Law,

The Early Life Research Unit,
Division of Child Health, Obstetrics and Gynaecology,
School of Medicine,
University Hospital,
University of Nottingham,
Nottingham, NG7 2UH United Kingdom
Telephone: +44 115 82 30611 Fax: +44 115 82 30626
Email: james.law@nottingham.ac.uk
Status: Assistant Professor in Child Health, doctor-in-training & PhD student.

Key terms: Brown adipose tissue, Thermal imaging, Infrared thermography, PET-CT,

Word count: 3616

Number of figures: 3

Number of tables: 4

Disclosure Statement: The authors have nothing to disclose

Acknowledgements:

The Section of Endocrinology and Investigative Medicine at Imperial College is funded by grants from the MRC, BBSRC, NIHR, an Integrative Mammalian Biology (IMB) Capacity Building Award, an FP7- HEALTH- 2009- 241592 EuroCHIP grant and is supported by the NIHR Biomedical Research Centre Funding Scheme. The views expressed are those of the author(s) and not necessarily those of any of the funders, the NHS, the NIHR or the Department of Health. VS is funded by a Diabetes UK Harry Keen Fellowship. WSD is funded by an NIHR Research Professorship.

Short Title: IRT vs PET-CT to assess human BAT

ABSTRACT

Background

Obesity and its metabolic consequences are a major cause of morbidity and mortality. Brown adipose tissue (BAT) utilises glucose and free fatty acids to produce heat, thereby increasing energy expenditure. Effective evaluation of human BAT stimulators is constrained by current standard BAT assessment methods as positron emission tomography-computed tomography (PET-CT) requires exposure to high doses of ionising radiation. Infrared thermography (IRT) is a potential non-invasive, safe alternative, although direct corroboration with PET-CT has not previously been established.

Methods

IRT and 18F-fluorodeoxyglucose (^{18}F-FDG) PET-CT data from 8 healthy male participants subjected to water jacket cooling were directly compared. Thermal images (TIs) were geometrically transformed to overlay PET-CT-derived maximum intensity projection (MIP) images from each subject and the areas of greatest intensity of temperature and glucose-uptake within the supraclavicular regions compared. Relationships between supraclavicular temperatures from IRT (T_{SCR}) and the maximum rate of glucose uptake (MR(gluc)) from PET-CT were determined.

Results

Glucose uptake on $MR(gluc)_{MIP}$ was positively correlated with change in T_{SCR} relative to a reference region (r^2 = 0.721; p=0.008). Spatial overlap between areas of maximal $MR(gluc)_{MIP}$ and maximal T_{SCR} was 29.5±5.1%. Prolonged cooling to 60 minutes was associated with further T_{SCR} rise compared with cooling to 10 minutes.

Conclusions

The supraclavicular hotspot identified on IRT closely corresponds to the area of maximal uptake on PET-CT-derived $MR(gluc)_{MIP}$ images. Greater increases in relative T_{SCR} were associated with raised glucose uptake. IRT should now be

considered a suitable method for measuring BAT activation, especially in populations where PET-CT is not feasible, practical or repeatable.

INTRODUCTION

Obesity is a leading global health concern, with no effective drug treatments currently available. An adverse metabolic profile, including insulin resistance and raised blood lipids, is a common pathway to many of the consequences of obesity. BAT is a major effector of adaptive thermogenesis and an attractive anti-obesity drug target (*1*). It is a highly metabolically active organ which utilises glucose and free fatty acids and is able to release chemical energy efficiently as heat by uncoupling mitochondrial respiration from adenosine triphosphate production (*2*). Increased BAT activity results in raised energy expenditure, improved glycaemic control and blood lipid profile (*3*).

In recent years, following its rediscovery in adult humans (*4-8*), BAT has been the focus of intense research. However, replication of the promising results from animal studies has been slow (*9*). This is due, in part, to difficulties measuring BAT activity directly in humans. Its variable anatomical position, close to major vessels, makes it difficult to safely biopsy routinely, resulting in imaging being the preferred method of BAT quantification. The standard method of BAT imaging remains PET-CT which exposes participants to significant radiation doses and is, therefore, not suitable for studies with repeated measures, large numbers of healthy volunteers, or children. It is also limited to making measurements in fasted subjects (*10*).

An alternative imaging technique, IRT, makes use of the heat emitting properties of BAT and the relatively superficial position of the supraclavicular depot, one of the largest BAT depots in adults (*7*). Using IRT, several research groups have shown a specific rise in T_{SCR} following introduction of a cool stimulus (*11-14*). IRT has the advantage of being able to measure real-time activation and can be used to gather repeated measures in large numbers of healthy subjects irrespective of age and nutritional status (*11*).

To date, IRT has not been validated against the current gold standard ^{18}F-FDG PET-CT. Whilst results from multiple previous IRT studies are consistent with the measurement of BAT, the lack of data directly comparing results between PET-CT and IRT in the same subjects has remained a limitation of the technique. Using novel IRT analysis methods and utilising additional PET-CT analysis techniques to those used by Salem et al. (*13*), the anatomical and functional relationship between alternative measures of BAT is explored in individual participants. We show here, for the first time, that the area identified as overlying BAT using IRT closely corresponds to the area of maximal glucose uptake on PET-CT and that the higher the glucose uptake on PET-CT the better the agreement.

MATERIALS AND METHODS

Subjects

In order to determine the correlation between BAT activity measured by PET-CT and IRT, 8 healthy men, known to be BAT positive on PET-CT (*13*) (mean age 23.5, range 18-35 years; mean body mass index 22.0, range 19.3-23.0 kg/m^2) underwent PET-CT and IRT sessions as part of a study approved by the London Central Ethics and Research Committee (13/LO/0925), registered with ClinicalTrials.gov (NCT01935791) and performed in accordance with the Declaration of Helsinki. Written informed consent was obtained from subjects before enrolment in the study. Participants who were BAT negative on the initial PET-CT scan (*13*) were not included in the analysis due to the small size of the group (n=3).

Study Visits

As previously described (*13*), participants attended an initial IRT session and initial PET-CT session. For both visits, volunteers wore a pair of light cotton trousers with a cooling vest surrounding the torso, away from the supraclavicular region. Following acclimatisation, cold water at 8°C (*13*) was pumped through the cooling vest to stimulate BAT.

In summary, during the thermal imaging session, images were captured during acclimatisation; over the first 10 minutes of cooling (initial period), which

represents the period of maximal BAT activation from resting state (*12*); and after prolonged stimulation (final period) (Fig. 1). Images were acquired using a FLIR T440bx infrared camera (FLIR Systems, West Malling, UK). During the PET-CT visit, 180MBq of ^{18}F-FDG was injected following water-vest cooling and a 60 minute dynamic emission scan was performed with an axial field of view from mandible to mid-thorax (*13*).

All volunteers attended a second thermal imaging session without cold stimulation (IRT vehicle session) and 4 volunteers who were BAT positive on the first PET-CT scan underwent a further PET-CT imaging session, without cold stimulation (PET-CT vehicle session). Thermal and PET-CT images were acquired as before.

Analysis of IRT

TIs acquired by IRT taken at 5 second intervals were analysed from each period of imaging for both IRT sessions. We developed a semi-automated method for analysis of TIs to allow the efficient analysis of large numbers of images in a systematic and reproducible manner by firstly converting the TIs to the non-proprietary Portable Network Graphic format, identifying the supraclavicular regions of interest (ROIs) and, finally, processing the data within the ROIs.

Conversion of the TIs was carried out using our custom-built Thermal-Imaging Technical Conversion Hub (TITCH), a Raspberry Pi™-based device, which extracts the raw data from the TI and saves it in an openly accessible format from which temperature data can be calculated (*15*,*16*). Our method for converting the raw radiometric data to temperature data produces identical results to that obtained by FLIR's proprietary software (data not shown).

Left and right supraclavicular ROIs were defined as previously described (*12*). In contrast to previous methods (*12*), this simply required each image (Fig. 2A) to be labelled with five key points, corresponding to the apices of the ROIs (Fig. 2B). The medial and inferior borders of the ROI were defined as straight lines between the appropriate apices. The contour of the neck was defined programmatically by identifying the temperature gradient between the volunteer

and the background. This represents a significant improvement on previously published methods, where the lateral border of the ROI is approximated to a simple straight line (*17*) or is painstakingly identified between manually plotted points (*12*).

The hottest ten percent of points within each ROI were identified and the medians of these points were calculated (*11*,*12*,*18*) (equivalent to the 95th percentile). Corresponding graphical output allowed clear visualisation of the identified hotspot (Fig. 2B). A reference region consisting of a circle, 10 pixels in diameter, immediately below the central apex of the ROIs was analysed for comparison. A moving average (period 5) was applied to the resulting time series to reduce the effect of natural variation in measurements. The main outcome measures for IRT were: base T_{SCR} (mean of the first minute of stimulation); peak T_{SCR} (maximal T_{SCR} within a given period); and ΔT_{SCR} (peak T_{SCR} – base T_{SCR}), all calculated for the right ROI (*11*) over the first 10 minutes of cooling relative to the reference region (*11*,*18*) . Secondary outcomes included analysis of absolute T_{SCR} values as well as comparison of left and right ROIs.

Videos of change in skin temperature over time, relative to the baseline image, were compiled. Pixels were averaged over three sequential images and sequential frames registered to the baseline image by applying an automatically calculated geometric transformation consisting of translation, rotation and scale. Unchanged pixels were displayed as white with colder pixels displayed as progressively blue then black, and warmer pixels as progressively red then yellow (Online Supplementary Fig.).

Analysis of PET-CT

Regional estimates of the metabolic rate of glucose [$MR(gluc)_{BAT}$] were calculated as previously described (*13*). In addition, two coronal MIP images for each volunteer were calculated from the PET-CT data for each visit, one for the CT image (CT_{MIP}) and one for the MR(gluc) values ($MR(gluc)_{MIP}$) (*19*). MIP images are 2-dimensional representations of 3-dimensional data, with the value of each point determined by the maximum intensity of the data along a point-line perpendicular to the projected plane, that is:

$CT_{MIP}(x,y) = max_z(CT(x,y,z))$, and

$MR(gluc)_{MIP}(x,y) = max_z(MR(gluc)(x,y,z))$.

A composite of the two MIP images was used in the graphical output (Fig. 2). The region of the greatest ten percent of $MR(gluc)_{MIP}$ was identified and the median of these values calculated for comparison with the results of IRT.

PET-CT / IRT Comparison

To identify similarities and differences between the data acquired from PET-CT and that acquired from IRT, the TI was warped onto the $MR(gluc)_{MIP}$ image from the same participant (Fig. 2). The comparative TI was a mean composite of the last three images from the initial imaging session (i.e. after 10 minutes of stimulation) (Figs. 2A and 2B). The TI and $MR(gluc)_{MIP}$ images were displayed beside each other and control point (cp) pairs were defined, identifying corresponding anatomical points. 70 cp pairs were identified the supraclavicular region of each pair of images, with additional non-supraclavicular points depending on the framing of the images. A locally weighted mean transformation (*20*) mapping was created by inferring a second degree polynomial at each cp based on the 16 closest points and using a locally weighted average of these polynomials. This mapping was applied to the TI (Fig. 2C).

An ROI was identified on the $MR(gluc)_{MIP}$ defined by applying the locally weighted mean transformation to the contour of the ROI of the TI and superimposing this on $MR(gluc)_{MIP}$. The greatest ten percent of values within the ROI were identified for the $MR(gluc)_{MIP}$ and the median of these points calculated in a similar manner to that described for the TI (Fig. 2D).

The percentage spatial overlap between TI and $MR(gluc)_{MIP}$ hotspots was calculated and displayed as an image (Fig. 2E). Since the TI and $MR(gluc)_{MIP}$ hotspots are, by definition, the same size, the overlap is the number of pixels that the hotspots have in common divided by the total number of pixels of either hotspot).

Statistical Analysis

Following conversion of the TI to the Portable Network Graphic format, further graphical analysis was carried out using MATLAB 2016a (The Mathworks Inc., Natick, MA, USA). The identification of the apices was undertaken using a custom-built graphic-user interface within MATLAB and a second script was written to undertake the analysis. The inbuilt MATLAB function *imregister* was used to register sequential images to compile the videos, *cpselect* was used to identify cp pairs and *fitgeotrans* was used to fit an lwm transformation object to the cp pairs. Analysis of trends in T_{SCR} over time and correlations between variables was undertaken using R: A Language and Environment for Statistical Computing v3.2.3 (R Core Team, Vienna, Austria).

RESULTS

TI Analyses

Analyses of TIs from the initial imaging period of the cooling session, showed that participants had a base T_{SCR} of 35.1±0.3 °C at the start of stimulation, with a peak temperature of 35.2±0.3 °C during the first 10 minutes of stimulation (change during first 10 minutes of stimulation ($\Delta_{10}T_{SCR}$): 0.1±0.03 °C) (Table 1a). Base T_{SCR} was 1.9±0.2 °C above the sternal reference region, with a peak difference of 2.2±0.3 °C during the first 10 minutes of stimulation ($\Delta_{10}T_{SCR}$: 0.3±0.05 °C) (Table 1b). Peak T_{SCR} of the initial imaging period alone was significantly lower than peak T_{SCR} during the initial and final imaging periods combined (initial only: 35.2±0.3 °C, both: 35.4±0.2 °C; p = 0.03). Similarly, mean T_{SCR} over the last minute of the initial period of stimulation was significantly lower than mean T_{SCR} over the last minute of the final imaging session (35.1±0.3 °C vs 35.3±0.2 °C respectively; p = 0.03).

There were trends towards lower base T_{SCR} from the vehicle compared with the cooling session (vehicle: 35.7±0.07 °C; cooling: 35.1±0.3 °C; p = 0.09) and lower peak T_{SCR} (vehicle: 35.8±0.06 °C; cooling: 35.2±0.3 °C; p=0.09) but no difference in $\Delta_{10}T_{SCR}$ (vehicle: 0.1±0.03 °C; cooling: 0.1±0.03 °C; p = 0.64). When compared to the reference region, however, base T_{SCR} (vehicle: 1.4±0.15 °C; cooling: 2.1±0.23 °C; p = 0.008), peak T_{SCR} (vehicle: 1.5±0.15 °C; cooling:

2.4±0.26 °C; p = 0.006) and $\Delta_{10}T_{SCR}$ (vehicle: 0.1±0.03 °C; cooling: 0.3±0.04 °C; p = 0.007) were all significantly increased by cooling.

Overlap

Representative images of the process are shown in Fig. 2. TI hotspots and $MR(gluc)_{MIP}$ hotspots were located in the same anatomical area of the ROIs (Fig. 2E). The overlap between the area of maximal glucose uptake on $MR(gluc)_{MIP}$ and the warmest pixels on TI was 29.5% respectively (range 11.6% to 55.5%, Table 2). Images from participants who underwent a PET-CT vehicle session demonstrated that, in the absence of cooling activation of BAT, the overlap between the hotspots was significantly less (cooling: 27.9±6.2% overlap; vehicle: 6.3±3.1% overlap; p = 0.009) (Table 2).

Relationship Between Hotspots on PET-CT and IRT

Linearity of the relationship between the IRT and PET-CT outcomes from cooling sessions are given in Table 3. There were strong positive correlations between relative $\Delta_{10}T_{SCR}$ and both $MR(gluc)_{MIP}$ (r^2 = 0.721; p = 0.008) and $MR(gluc)_{BAT}$ (r^2 = 0.583; p = 0.027). Absolute T_{SCR} measurements and relative base and peak T_{SCR} did not significantly correlate with $MR(gluc)_{MIP}$ or $MR(gluc)_{BAT}$.

All 4 participants who had both cold-activated and vehicle PET-CT scans had an increase in both relative $\Delta_{10}T_{SCR}$ and $MR(gluc)_{MIP}$ during cooling compared to the control session (Fig. 3).

Stronger correlations were seen between the right ROI and PET-CT outcomes than the left ROI (Table 4). The left ROI demonstrated a strong positive correlation between $MR(gluc)_{MIP}$ and relative $\Delta_{10}T_{SCR}$ (r^2 = 0.698, p = 0.010) but not with other relative IRT outcomes or with $MR(gluc)_{BAT}$.

DISCUSSION

IRT is increasingly being used to assess BAT activation and has established an important role in imaging of healthy volunteers, children, for repeat imaging and in studies not conducted in the fasted state (*10*). These are all situations where exposure to ionising radiation must be minimised. Despite this, the definitive

evidence that IRT measures BAT activity has been lacking. Even studies that have utilised both techniques have done so in a way that does not allow direct comparison (*21*). We demonstrate here, for the first time, that there is anatomical overlap of the area of maximum temperature measured using IRT and the projected area of maximum glucose uptake on PET. IRT correlates strongly with MR(gluc) from PET-CT. Indeed, since ^{18}F-FDG PET-CT measures glucose uptake and not thermogenic capacity per-se (*22*), greater correlations would not reasonably be expected.

PET-CT thus makes a different measure of BAT function compared with IRT i.e. glucose uptake as opposed to heat production. Which of these measures is the optimum index of BAT function remains to be fully clarified. We observed that subjects which are BAT positive as determined by PET-CT exhibit a similar magnitude of BAT function with IRT. It should be further noted that PET-CT is usually conducted in fasted subjects as after feeding the uptake in BAT is largely masked by the much greater uptake in skeletal muscle (*10*). Feeding per se has been suggested to stimulate BAT function (*23*) and, to date, we have been able to detect a positive IRT in all subjects measured (n>200). Taken together these findings indirectly support those from repeated PET-CT in which a majority of subjects appear to be BAT positive in at least one scan (*24*). In addition, as with the reduced BAT activity in obese adults as measured with PET-CT (*25*) we have previously observed a reduction in BAT activity with increasing BMI percentile in children (*11*). Future work comparing differences between IRT and PET-CT measures may indeed offer novel insights into different components of BAT activation.

Previous papers have often used absolute T_{SCR} as the primary outcome. However, there are many factors which may affect this and can even cause it to fall (*18*). In many cases, the magnitude of the effect on T_{SCR} is sufficient to overcome any counteracting factors, but it is clear that true, relative warming is best demonstrated by comparing the T_{SCR} to a reference region. We have used a region on the sternum, but alternatives, such as mean skin temperature (*18*), may allow more subtle effects to be revealed. However, even with the addition of

a simple reference region, the true relationship between the two measures of BAT activity becomes evident. This is perhaps not surprising when videos of change in skin temperature relative to baseline are viewed (Online Supplementary Fig.). These show the specific warming of the supraclavicular region relative to surrounding skin temperatures and, therefore, the importance of framing the participant to include the superior portion of the sternum as a reference.

We have previously seen a greater rise in the T_{SCR} of the right ROI (*11*). In addition, we show here that the outcome measures using the right ROI correlate better with BAT glucose uptake on PET-CT than the left ROI or a combined measure. The reasons for this merit further investigation and could be due to either anatomical or functional differences. There is no evidence of a difference between the volume of BAT on the left and right on PET-CT (*26*) but functional symmetry has not been investigated in non-IRT modalities which could reveal whether it is a true difference in activity or, for instance, an artefact or example of the slightly different anatomical positions of BAT on the left and right.

Base T_{SCR} was measured as an average of the first minute of stimulation. That this is already higher in participants during the cold session demonstrates the rapid nature of the BAT response of cold stimulus. We show here that the response seen within the first 10 minutes is sufficient to ascertain an individual's BAT activity, correlating well with glucose uptake on PET-CT but, contrary to previous reports (*12*), prolonged stimulation is associated with further rise in T_{SCR}. In addition, a proper acclimatisation period is essential for the accurate measurement of BAT activity using IRT and our data (not published) show that this should be 20 minutes during which time the participant should be in the same environment and clothing as for the study and remain as still as during imaging.

The area of maximal glucose uptake on a coronal projection MIP image from ^{18}F-FDG PET-CT closely corresponds to the warmest area within the supraclavicular ROI measured using IRT. In the eight participants, known to be BAT positive on

PET-CT, a high degree of overlap was demonstrated between the most intense glucose uptake on PET-CT and the warmest area on IRT.

The main limitation of these analyses is the small number of participants available, reducing the power to detect correlations between IRT and PET-CT outcomes. Larger studies are not ethical feasible, especially in healthy volunteers, due to the risks of exposure to the ionising radiation associated with PET-CT. We recommend that studies using IRT to measure BAT activity should report the right ROI relative to a reference region, and authors should include a statement about the acclimatisation period to which participants were exposed.

Advances in IRT are allowing a more detailed assessment of the changes in superficial temperature associated with underlying BAT changes to be made. Radiometric sensors are becoming increasingly accurate, with some sensors now able to distinguish changes of 0.01°C and the resolution of images is improving, with cameras able to take truly high definition images. These improvements will allow the subtler changes to be better defined, especially when combined with more sophisticated mean skin temperature reference calculations. In order to take full advantage of these improvements, together with those in image acquisition rates, a fully automated analysis method should be considered. In addition, an automated standardised analysis method would reduce variability between groups. The establishment of IRT as a valid method of measuring supraclavicular BAT activity in humans will make studies feasible that until now have not been possible.

CONCLUSION

IRT can provide a safe, credible and quantifiable alternative to PET-CT for the measurement of BAT activity that can now be used in a wide range of population groups.

REFERENCES

1. Chechi K, Nedergaard J, Richard D. Brown adipose tissue as an anti-obesity tissue in humans. *Obes Rev.* 2014;15:92-106.

2. Cannon B, Nedergaard J. Brown adipose tissue: function and physiological significance. *Physiol Rev.* 2004;84:277-359.

3. Sidossis L, Kajimura S. Brown and beige fat in humans: thermogenic adipocytes that control energy and glucose homeostasis. *J Clin Invest.* 2015;125:478-486.

4. Sacks HS. The importance of brown adipose tissue. *N Engl J Med.* 2009;361:author reply 418-420.

5. Celi FS. Brown adipose tissue--when it pays to be inefficient. *N Engl J Med.* 2009;360:1553-1556.

6. Virtanen KA, Lidell ME, Orava J, et al. Functional brown adipose tissue in healthy adults. *N Engl J Med.* 2009;360:1518-1525.

7. Cypess AM, Lehman S, Williams G, et al. Identification and importance of brown adipose tissue in adult humans. *N Engl J Med.* 2009;360:1509-1517.

8. van Marken Lichtenbelt WD, Vanhommerig JW, Smulders NM, et al. Cold-activated brown adipose tissue in healthy men. *N Engl J Med.* 2009;360:1500-1508.

9. Roman S, Agil A, Peran M, et al. Brown adipose tissue and novel therapeutic approaches to treat metabolic disorders. *Transl Res.* 2015;165:464-479.

10. Vosselman MJ, Brans B, van der Lans AA, et al. Brown adipose tissue activity after a high-calorie meal in humans. *Am J Clin Nutr.* 2013;98:57-64.

11. Robinson L, Ojha S, Symonds ME, Budge H. Body mass index as a determinant of brown adipose tissue function in healthy children. *J Pediatr.* 2014;164:318-322.

12. Symonds ME, Henderson K, Elvidge L, et al. Thermal imaging to assess age-related changes of skin temperature within the supraclavicular region co-locating with brown adipose tissue in healthy children. *J Pediatr.* 2012;161:892-898.

13. Salem V, Izzi-Engbeaya C, Coello C, et al. Glucagon increases energy expenditure independently of brown adipose tissue activation in humans. *Diabetes Obes Metab.* 2016;18:72-81.

14. Lee P, Ho KK, Lee P, Greenfield JR, Ho KK, Greenfield JR. Hot fat in a cool man: infrared thermography and brown adipose tissue. *Diabetes Obes Metab.* 2011;13:92-93.

15. Tattersall GJ. Infrared thermography: A non-invasive window into thermal physiology. *Comp Biochem Physiol, Part A Mol Integr Physiol.* 2016;202:78-98.

16. *Thermimage: Functions for Handling Thermal Images. R package version 1.0.1.* [computer program]. Version; 2015.

17. Gatidis S, Schmidt H, Pfannenberg CA, Nikolaou K, Schick F, Schwenzer NF. Is it possible to detect activated brown adipose tissue in humans using single-time-point infrared thermography under thermoneutral conditions? Impact of BMI and subcutaneous adipose tissue thickness. *PLoS One.* 2016;11:e0151152.

18. Robinson LJ, Law JM, Symonds ME, Budge H. Brown adipose tissue activation as measured by infrared thermography by mild anticipatory psychological stress in lean healthy females. *Exp Physiol.* 2016;101:549-557.

19. Wallis JW, Miller TR, Lerner CA, Kleerup EC. Three-dimensional display in nuclear medicine. *IEEE Trans Med Imaging.* 1989;8:297-230.

20. Goshtasby A. Image registration by local approximation methods. *Image Vis Comput.* 1988;6:255-261.

21. Ramage Lynne E, Akyol M, Fletcher Alison M, et al. Glucocorticoids acutely increase brown adipose tissue activity in humans, revealing species-specific differences in UCP-1 regulation. *Cell Metab.* 2016;24:130-141.

22. Olsen JM, Csikasz RI, Dehvari N, et al. β3-adrenergically induced glucose uptake in brown adipose tissue is independent of UCP1 presence or activity: mediation through the mTOR pathway. *Mol Metab.* 2017;6:611-619.

23. Scotney H, Symonds ME, Law J, Budge H, Sharkey D, Manolopoulos KN. Glucocorticoids modulate human brown adipose tissue thermogenesis in vivo. *Metab Clin Exp.* 2017;70:125-132.

24. Lee P, Smith S, Linderman J, et al. Temperature-acclimated brown adipose tissue modulates insulin sensitivity in humans. *Diabetes.* 2014;63:3686-3698.

25. Vijgen GH, Bouvy ND, Teule GJ, Brans B, Schrauwen P, van Marken Lichtenbelt WD. Brown adipose tissue in morbidly obese subjects. *PLoS ONE.* 2011;6:e17247.

26. Jang C, Jalapu S, Thuzar M, et al. Infrared thermography in the detection of brown adipose tissue in humans. *Physiol Rep.* 2014;2:e12167.

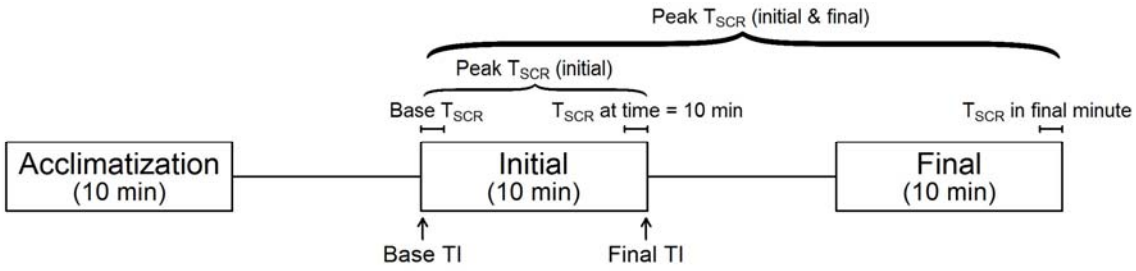

Figure 1 IRT imaging protocol annotated with IRT outcomes
Acclimatisation: Imaging period during acclimatisation; Initial: imaging period during first 10 minutes of stimulation; Final: imaging period following stimulation for ~1 hour. TI: thermal image, T_{SCR}: supraclavicular temperature. $\Delta_{10}T_{SCR}$: change in T_{SCR} (peak T_{SCR} – base T_{SCR}) over the first 10 minutes of cooling

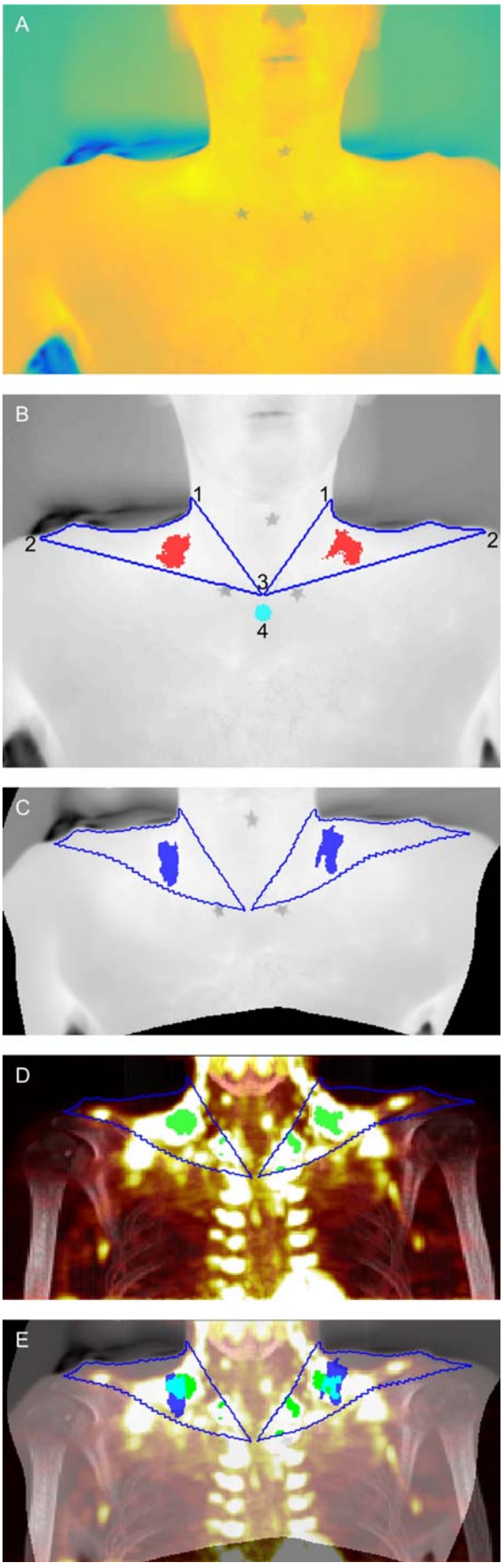

Figure 2 Summary of the process of mapping TI to PET-CT

(A) Apices of the ROIs are identified on the original TI. (B) Contour of ROI (blue) and hottest 10% pixels (red) identified, with contour of neck precisely defined using automated process. 1. Left and right superolateral apices; 2. Acromioclavicular apices; 3. Sternal apex; 4. Reference area (C) TI following warping by lwm transformation calculated following identification of cp pairs. (D) Warped contour superimposed on MIP with most intense 10% pixels highlighted (green). (E) Final composite image with warped TI superimposed on MIP image and hottest pixels from TI (blue), most intense pixels from MIP (green) and overlap (cyan) demonstrating close anatomical proximity

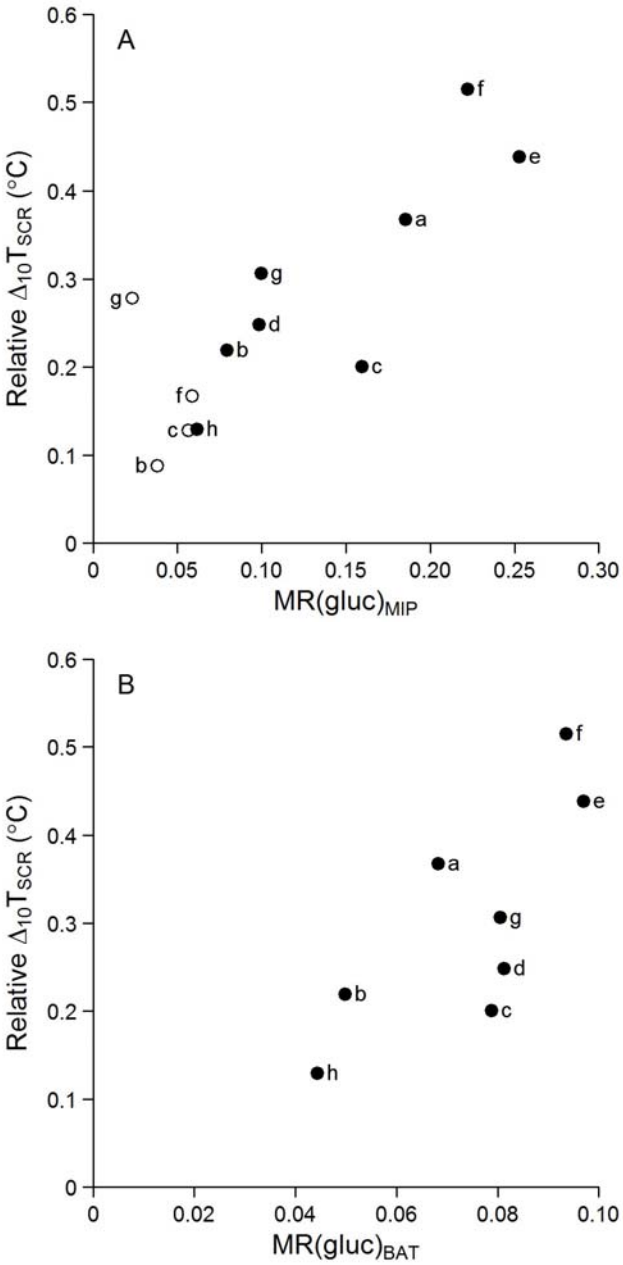

Figure 3 Δ_{10} T_{SCR} (relative to sternal reference) against glucose uptake on PET-CT by (A) MR(gluc)$_{MIP}$ and (B) MR(gluc)$_{BAT}$

Correlation between glucose uptake measured on PET-CT and the relative change in supraclavicular temperature over the first 10 minutes of stimulation ($\Delta_{10}T_{SCR}$) showing correlation between BAT activity measured with IRT and (A) the median MR(gluc)$_{MIP}$ hotspot value (r^2 = 0.721; p=0.008); and (B) MR(gluc)$_{BAT}$ (r^2 = 0.583; p = 0.027). Open: control; filled: cooling. MIP: maximum intensity projection; MR(gluc): metabolic rate of glucose; PET-CT: positron emission tomography-computed tomography; T_{SCR}: supraclavicular temperature.

Table 1 Summary of outcomes of IRT analysis (A) Absolute T_{SCR} and (B) Relative T_{SCR} to a sternal reference region.

A	**Absolute T_{SCR} (°C)**		
	Vehicle session	Cold Session	p-value
Base T_{SCR}	35.7±0.07	35.1±0.29	0.09
Peak T_{SCR} (initial)	35.8±0.06	35.2±0.29	0.09
$\Delta_{10}T_{SCR}$	0.1±0.03	0.1±0.03	0.64
Peak T_{SCR} (initial & final)	35.9±0.08	35.4±0.25	0.06
T_{SCR} at 10mins of cooling	35.6±0.07	35.1±0.30	0.11
T_{SCR} in final minute of cooling	35.7±0.08	35.3±0.25	0.09

B	**T_{SCR} relative to sternal reference region (°C)**		
	Vehicle session	Cold Session	p-value
Base T_{SCR}	1.3±0.13	1.9± 0.24	0.01
Peak T_{SCR} (initial)	1.4±0.13	2.2±0.27	0.01
$\Delta_{10}T_{SCR}$	0.2±0.03	0.3±0.05	0.04
Peak T_{SCR} (initial & final)	1.5±0.14	2.7±0.29	0.001
T_{SCR} at 10mins of cooling	1.4±0.14	2.2±0.26	0.004
T_{SCR} in final minute of cooling	1.4±0.13	2.6±0.27	0.0004

Means (± SEM) from 8 adult males. T_{SCR}: supraclavicular temperature; $\Delta_{10}T_{SCR}$: change in T_{SCR} (peak T_{SCR} – base T_{SCR}) over the first 10 minutes of cooling

Table 2 Percentage spatial overlap between MIP and TI

Individual values from 8 adult males showing the percentage spatial overlap between the area of maximum supraclavicular MR(gluc) on the $MR(gluc)_{MIP}$ image and the area of maximum supraclavicular temperature on the TI. Overlap for participants who underwent both cold and vehicle PET-CT scans was significantly reduced in the vehicle sessions (cold: 35.4±5.1%, vehicle: 4.7±2.8%, $p < 0.001$).

Participant	Overlap (%)	
	Cold	Vehicle
A	31.6	
B*	11.6	0.1
C*	36.6	8.4
D	55.5	
E	14.3	
F*	38.5	14.1
G*	24.9	2.6
H	22.9	
Mean±SEM	29.5±5.1	
Mean±SEM (*)	27.9±6.2	6.3±3.1

MIP: maximum intensity projection; MR(gluc): Metabolic rate of glucose; SEM: Standard error of the mean; TI: Thermal image.

Table 3 Correlation between IRT outcome variables and PET-CT measures

	IRT Outcome (right ROI)	$MR(gluc)_{MIP}$	$MR(gluc)_{BAT}$
Relative	Base T_{SCR}	0.280 (ns)	0.003 (ns)
	Peak T_{SCR} (initial)	0.386 (ns)	0.032 (ns)
	$\Delta_{10}T_{SCR}$	0.721**	0.583*
Absolute	Base T_{SCR}	0.118 (ns)	0.443^
	Peak T_{SCR} (initial)	0.087 (ns)	0.406^
	$\Delta_{10}T_{SCR}$	0.214 (ns)	0.056 (ns)

Values are r^2, the square of the Pearson's coefficient for the 8 male volunteers. BAT: brown adipose tissue; IRT: infrared thermography; MR(gluc): metabolic rate of glucose; MIP: maximum intensity projection; PET-CT: positron emission tomography-computed tomography; ROI: region of interest; T_{SCR}: supraclavicular temperature; $\Delta_{10}T_{SCR}$: change in T_{SCR} (peak T_{SCR} – base T_{SCR}) over the first 10 minutes of cooling ^p<0.1, *p<0.05, **p<0.01.

Table 4 Correlations between IRT outcome measures for left and right ROIs and PET-CT measures

PET-CT Outcome	IRT Outcome (relative to reference region)	Left ROI	Right ROI
$MR(gluc)_{MIP}$	Base T_{SCR}	0.172 (ns)	0.280 (ns)
	Peak T_{SCR} (initial)	0.239 (ns)	0.386*
	$\Delta_{10}T_{SCR}$	0.698**	0.721**
$MR(gluc)_{BAT}$	Base T_{SCR}	0.001 (ns)	0.003 (ns)
	Peak T_{SCR} (initial)	0.002 (ns)	0.032 (ns)
	$\Delta_{10}T_{SCR}$	0.337 (ns)	0.583*

Values are r^2, the square of the Pearson's coefficient for the 8 male volunteers. IRT: infrared thermography; Δ: change; PET-CT: positron emission tomography-computed tomography; ROI: region of interest; T_{SCR}: supraclavicular temperature; $\Delta_{10}T_{SCR}$: change in T_{SCR} (peak T_{SCR} – base T_{SCR}) over the first 10 minutes of cooling. ^p<0.1, *p<0.05, **p<0.01.

Online Supplementary Figure

Representative example of video showing the relative sparing of the supraclavicular region with respect to maintaining its temperature over time in response to a cold stimulus. Each frame is comprised of a rolling average of three consecutive images. Using the first frame as a reference, each consecutive frame is transformed (via translation, rotation, and scale) on to the first and compared to it. Areas that are the same temperature as the reference image are white; areas that are increasingly warmer than the original are red through orange to yellow; and areas that are increasingly cooler than the original are blue through to black.

The Journal of NUCLEAR MEDICINE

Thermal imaging is a non-invasive alternative to PET-CT for measurement of brown adipose tissue activity in humans

James Matthew Law, David Edward Morris, Chioma Izzi-Engbeaya, Victoria Salem, Christopher Coello, Lindsay Robinson, Maduka Jayasinghe, Rebecca Scott, Roger Gunn, Eugenii Rabiner, Tricia Tan, Waljit Dhillo, Stephen Bloom, Helen Budge and Michael Symonds

J Nucl Med.
Published online: September 14, 2017.
Doi: 10.2967/jnumed.117.190546

The Journal of Nuclear Medicine is published monthly.
SNMMI | Society of Nuclear Medicine and Molecular Imaging
1850 Samuel Morse Drive, Reston, VA 20190.
(Print ISSN: 0161-5505, Online ISSN: 2159-662X)

SNMMI SOCIETY OF NUCLEAR MEDICINE AND MOLECULAR IMAGING